LA-UR-01-6144
Approved for public release;
distribution is unlimited.

Title: **Pulsed Laser Beam Welding of 304 to 304L Stainless Steel: Effects of Welding Parameters on Cracking and Phase Transformations**

Author(s): Patrick W. Hochanadel, Mark J. Cola, Ann M. Kelly and Pallas A. Papin

Submitted to:

Pulsed Laser Beam Welding of 304 to 304L Stainless Steel: Effects of Welding Parameters on Cracking and Phase Transformations

Patrick W. Hochanadel, Mark J. Cola, Ann M. Kelly and Pallas A. Papin
MST-6: Metallurgy
Los Alamos National Laboratory
Los Alamos, NM 87545

Abstract

A series of annulus welds were made between 304 and 304L stainless steel coaxial tubes using pulsed laser beam welding (LBW). A processing map was constructed and cracking was found to occur at higher average (and peak) weld powers, while at lower powers, incomplete fusion was observed. The material compositions were predicted to be, by themselves, "weldable" according to the modified Suutala diagram[1]. However, by welding the two materials together, a composition range was predicted to be crack susceptible according to the aforementioned diagram. Microstructurally, the primary solidification mode (PSM) of higher power welds was determined to be austenite, while lower power welds exhibited a dual PSM of both austenite and ferrite-austenite within the same weld. Two factors were believed to contribute to the cracking: (1) a shift in the PSM from ferrite-austenite to austenite given the combination of compositions and higher growth rate during higher power welds and (2) higher thermal shock conditions of the higher power pulses. This work demonstrates that variations in crack susceptibility may be realized when welding different heats of "weldable" materials together, and that slight variations in processing can also contribute to crack susceptibility.

Introduction

Solidification cracking has been observed in austenitic stainless steel welds for quite some time. The correlation between the cracking and the primary solidification mode (PSM) has been studied extensively[1-9]. In many cases, the correlations have been observed in the case of simulative weldability tests such as Varestraint tests[10] or in other autogenous weld tests such as bead on plate welds, as in the case of the Suutala diagram[1,5,10]. Constitution diagrams have also been used extensively to predict the resulting microstructures in welds and have proved to be useful in selecting filler metals and/or predicting the resulting weld metal compositions in these welds[11-14]. Other studies have documented the cracking susceptibility in dissimilar metal welds[15]. In many instances, however, similar materials may be welded with a great amount of confidence in weld integrity. At times, however, a process change (such as gas tungsten arc to laser beam welding) or minor differences in the compositions of the heats of materials may provide an increase in cracking susceptibility that may not otherwise be predicted. An example of this was found when laser beam welding 304 to 304L stainless steel, which was historically done with gas tungsten arc welding (GTAW). The purpose of this investigation was to determine the cause for an increase in the cracking susceptibility of this seemingly similar metal joint in terms of welding process and microstructural evolution.

Procedure

Several annulus welds were made between 304L (outer tube) and 304 (inner tube) materials with LBW (see Figure 1). The 304L outer tube was machined from bar stock and the 304 inner tube was purchased as seamless tube material. Table I lists the nominal chemical composition of the materials investigated. Figure 1 shows the weld joint and centered position of the laser beam as well as the finished weld. A Lumonics JK706 Nd:YAG pulsed laser welder was used to make the weld. The average welding power ranged from 35 watts to 110 watts (verified by a calorimeter), and the pulse widths investigated were either 3ms or 5ms, giving a duty cycle of 3 percent or 5 percent, since the pulse frequency was held constant at 10 Hz. The travel speed was held constant at 0.5 mm/s, and the beam diameter was approximately 1 mm. All welds were made at sharp visual focus. Leak checking of the welds was performed with an Alcatel ASM 180t leak detector. Subsequent microstructural observation was performed after sectioning and polishing using standard metallographic procedures. Electrolytic etching was performed with a 10 pct. oxalic acid solution. Electron probe microanalysis (EPMA) was performed with a JEOL 840 at 15 kV and 20 nA to determine whether the composition changed significantly across the weldment.

	Outer Tube	Inner Tube
Cr	18.5	18.4
Ni	11.6	9.2
Mn	1.6	1.7
Si	0.36	0.49
Co	0.025	N/A
Mo	0.044	N/A
C	0.027	0.041
S	0.002	0.024
P	0.010	0.023
N	0.037	N/A
Fe	Bal.	Bal.

Table I. Nominal alloy compositions (in weight percent).

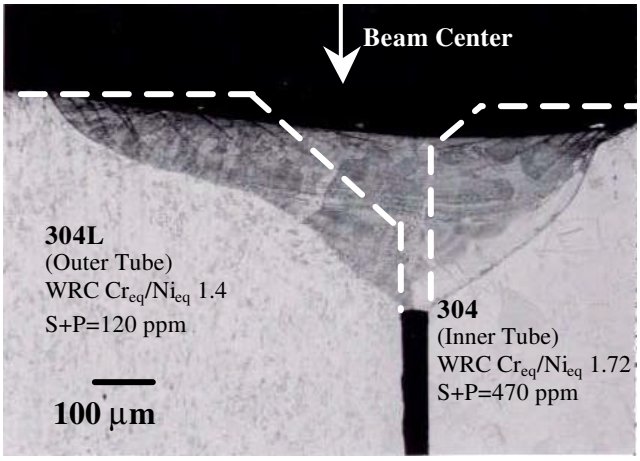

Figure 1. Cross-section of weldment and joint schematic (dashed lines) of the 304 to 304L stainless steel combination. Average power of the weld was 45 watts and the pulse width was 5ms.

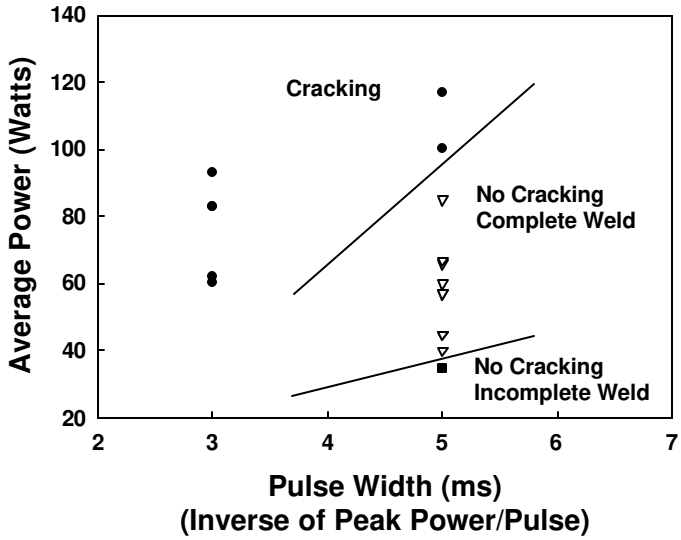

Figure 2. Processing map of power versus pulse width for pulsed laser beam welding of concentric tubes.

Results and Discussion

The resulting welds were found to either pass (at intermediate average welding powers) or fail (at low and high average welding powers) the leak check. Figure 2 shows a processing map for the weld with average power versus pulse width for the laser weld. It was easily seen (with visual inspection) that the lower power welds did not have a complete weld (Figure 3). At the higher power welds, however, visual inspection did not reveal anything useful. Metallography showed that these welds had significant solidification cracking throughout the weld, as shown in Figure 4. Although many of the cracks were found to be in the final weld pulse, cracks were found throughout the weld. By plotting the compositional window of the 304 or 304L stainless steels on a constitution diagram, as Lippold did in earlier work[15], it is easily seen that several resulting solidification microstructures may be realized depending upon the material compositions. This is seen in Figure 5. This figure also shows the compositions of interest plotted for comparison. It has been shown that 5 to 35 % delta ferrite produces crack resistant weld deposits[2], and the constitution diagram in Figure 5 predicts that the combination of these two materials are close to the 5 percent level. The Suutala diagram was modified by Lippold to display cracking tendencies in laser welded materials[1]. This is shown in Figure 6. In addition, the two compositions investigated in the current study were plotted as total S + P + B and Cr_{eq}/Ni_{eq}. This diagram shows clearly that both materials are readily weldable if they are welded autogenously. However, by placing a tie line between the two compositions, a region is found where the combination of these materials can yield a crack susceptible composition.

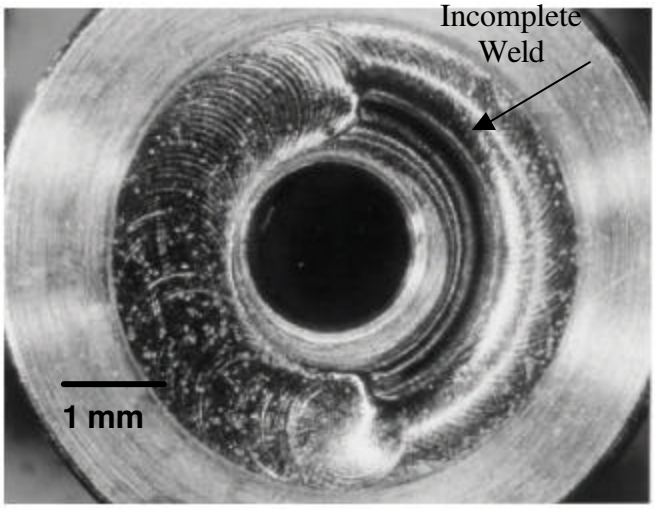

Figure 3. Photograph of incomplete weld processed at low power (35 watts average and 5 ms pulse width).

Lippold[1], Elmer, *et al.*[16], and David *et al.*[17] have shown that a material that is predicted to have a PSM of ferrite-austenite may solidify as primary austenite at higher solidification rates, as shown in Figure 7. In fact, this was Lippold's premise when developing an understanding of why the cracking curve is shifted from the left to the right in the Suutala diagram when employing high energy density welding processes[1]. In the current investigation, the resulting lower power welds show a bimodal solidification (solidification as both primary austenite on one side and primary ferrite on the other, as seen in the micrograph) in the 304 to 304L weld joint, as shown in Figure 8.

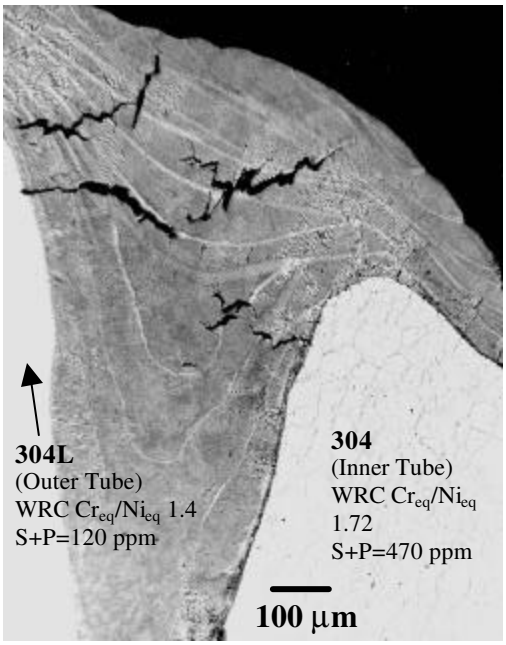

Figure 4. Solidification cracking along solidification grain boundaries in a higher power weld (95 watts average power and 3 ms pulse width).

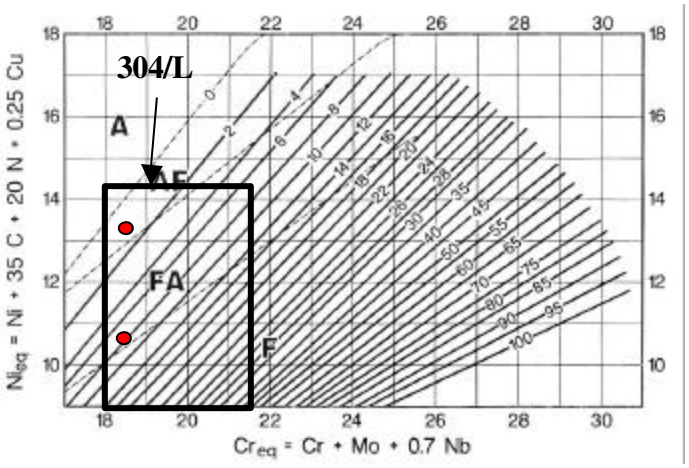

Figure 5. WRC-1992 diagram[14] showing the range for 304/L stainless steel composition. The two points are shown for the composition of materials investigated in the current study.

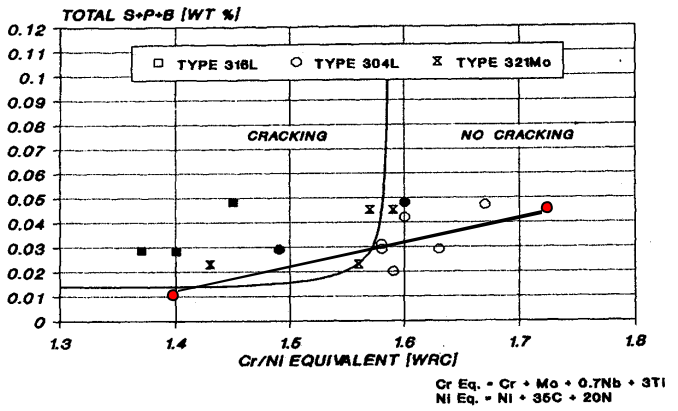

Figure 6. Modified Suutala diagram (adapted from Lippold[1]) showing tie-line between two compositions of interest.

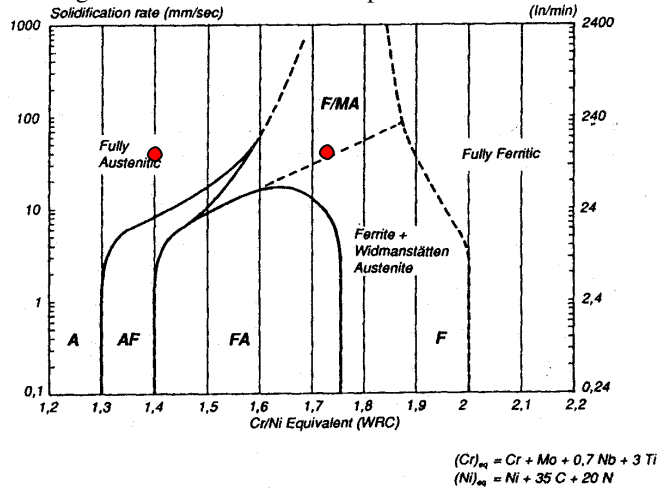

Figure 7. Solidification map showing the dependence of PSM on solidification rate and composition (adapted from Lippold[1]). The two compositions of interest are shown.

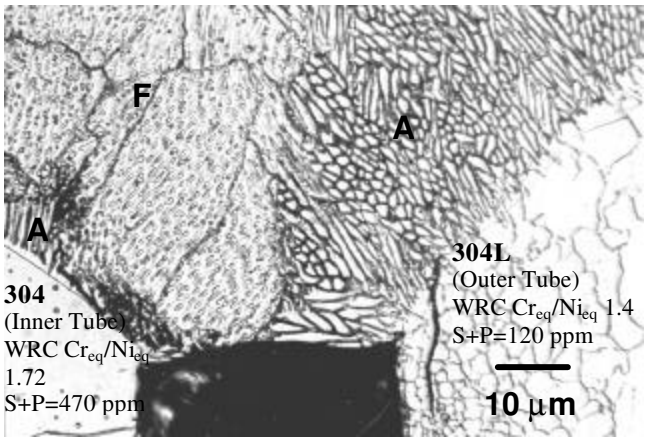

Figure 8a. Micrograph depicting the variation in solidification microstructure at the root of the weld. Adjacent regions of primary austenite (A) and primary ferrite (F) solidification are seen in a lower power weld (45 W average power and 5ms pulse width).

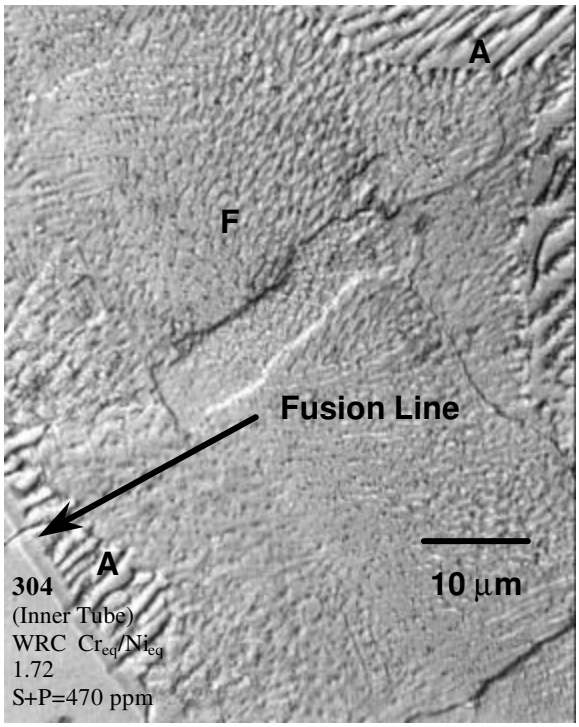

Figure 8b. Fusion boundary region depicting the heat affected zone, unmixed zone and transition regions. Note mixed primary solidification modes in a lower power weld (same parameters as 8a).

Figure 8 shows how epitaxial nucleation of primary austenite occurred initially upon solidification for a short distance, until the solidification mode shifted to primary ferrite (both in the root in Figure 8a and along the fusion boundary in 8b) . This phenomena was also observed by Lippold when pulsed laser welding austenitic stainless steels [1], and he surmised that the diffusion controlled transformation of austenite to ferrite in the heat affected zone was suppressed, allowing for epitaxial nucleation of austenite. Figure 8 also shows how the solidification mode changed back to primary austenite, as depicted by the "A" on the right-hand side of the micrographs. This could be caused by either a change in solidification growth rate, a change in composition (as expected), or a combination of both.

Figure 9 shows the fusion zone in the higher power weld. It appears that this higher power weld had only a primary solidification mode of austenite or austenite/eutectic ferrite (no evidence for primary ferrite solidification was observed).

Figure 10 shows the results of the EPMA across a weld exhibiting a bimodal solidification structure. Figure 10a shows the results for manganese, nickel, iron and chromium, while Figure 10b shows the composition profile for nickel alone. It was expected, based upon the light microscopy that an unmixed zone or region of higher Cr_{eq}/Ni_{eq} (nickel of about 9.5 weight percent) was to be observed with the EPMA. However, it was found that the weld metal composition is not uniform at all. In fact, the presence of an unmixed zone is adjacent to the fusion zone, and non-uniform mixing was observed adjacent to the unmixed zone. It was seen that a region of higher nickel (approximately 12 percent) was found adjacent to the unmixed zone. The nickel composition was similar to that of the 304L outer tube (lower Cr_{eq}/Ni_{eq}). Note that the chromium amount was not observed to change. Recall the WRC Cr_{eq}/Ni_{eq} of the outer tube is 1.4. Even with the higher austenite potential, the primary solidification mode of the material remained ferrite for a small distance, prior to changing back to primary austenite. Although the solidification potential changed from primary ferrite to primary austenite, the nucleation of primary austenite had to occur, and this did for a short distance after the solidification potential had changed.

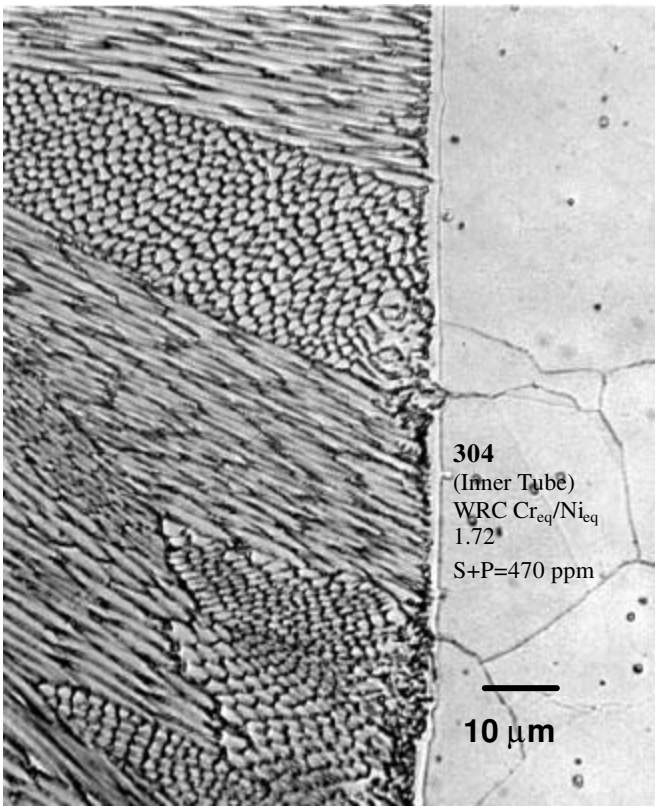

Figure 9. Fusion zone in a higher power weld (95 W average power and 3 ms pulse width) showing epitaxial growth and primary austenite solidification along the high Cr_{eq}/Ni_{eq} boundary of the inner tube.

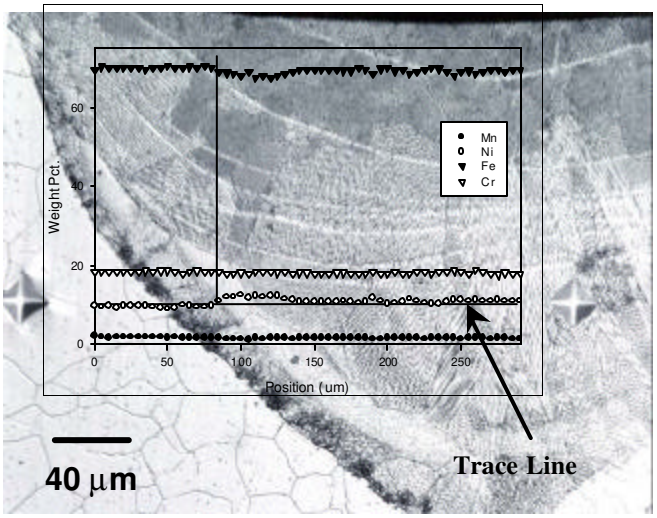

Figure 10a. EPMA results for 304 to 304L stainless steel weld showing manganese, nickel, iron and chromium in a lower power weld (45 W average power and 5 ms pulse width).

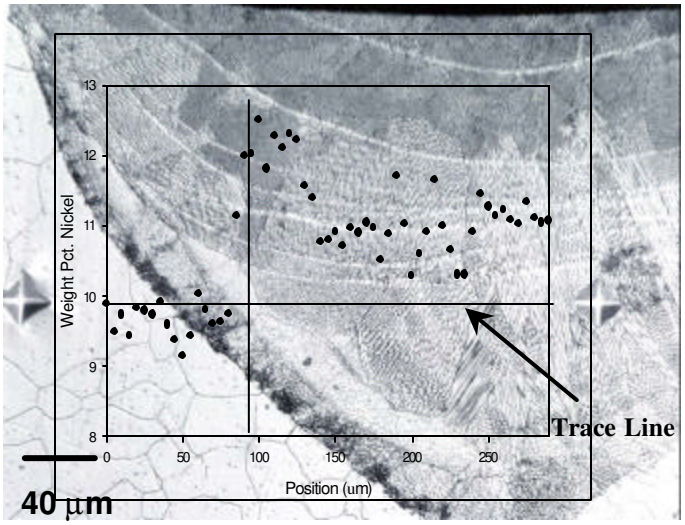

Figure 10b. EPMA results for 304 to 304L stainless steel weld showing only nickel (same weld as shown in Figure 10a).

Figure 11 shows the results of the EPMA across a higher power weld which exhibited either a primary austenite solidification or primary austenite/eutectic ferrite solidification. This figure has quite different results compared to the results of Figure 10. The composition of the higher power weld was found to abruptly change at the fusion line (from approximately 9.2 weight percent nickel to approximately 11.5 weight percent nickel, and no unmixed zone was discernable (visually or compositionally). The weld metal composition was observed to be much more uniform across the EPMA trace, and the WRC Cr_{eq}/Ni_{eq} was approximately that of the outer tube material (about 1.4). Also the chromium content of the weld metal was found to vary from about 18.7 weight percent in the base metal to about 17.5 weight percent in the weld metal.

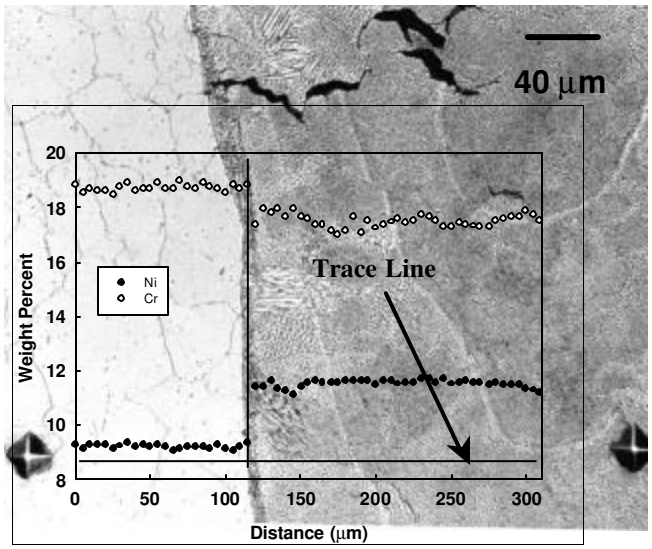

Figure 11. EPMA results for 304 to 304L stainless steel weld showing nickel and chromium in a higher power weld (95 W average power and 3 ms pulse width). Note lack of unmixed zone in this keyhole mode weld.

In the higher power welds (>75 watts average power with 5ms pulse), the welds were found to be keyhole mode welds, while at powers lower than 75 watts, conduction mode welds were observed. Possible causes for the solidification mode observations were either the difference in cooling rates between the two weld modes (conduction mode versus keyhole mode), the difference in mixing, or a combination of both.

A first order approximation of the cooling rate was shown first by Katayama and Matsunawa[18] and then by Elmer, *et al.*[16] to be predicted by the following

$$\lambda_1 = 80(\varepsilon)^{-0.33} \qquad (1)$$

where λ_1 is the cell spacing (in μm) and ε is the cooling rate (in K/s). The cooling rate was not found to vary much between the lower power welds and the higher power weld (*i.e.* conduction mode versus keyhole mode), all of which were determined to be on the order of 10^5 K/s. This is in good agreement with the predicted cooling rates reported in literature for pulsed laser welds[18,19]. Thus, it was determined that the cooling rate did not influence the observed change in solidification mode.

Based upon the results of the EPMA, the mixing was determined to have the greatest influence on the solidification mode, since the composition variations in the conduction mode weld allowed for a sizable unmixed zone (approximately 35 μm) and nonuniform mixing. The keyhole mode is a potent mode for rigorous mixing in the weld metal, as shown by the EPMA results, and as such, allowed for the use of the modified Suutala diagram and for a more uniform weld metal composition, which resulted in a more uniform weld metal microstructure. However, caution should be used in simply looking just at the

composition and general cooling rate data. Zacharia, *et al*.[19] have shown that local variations in cooling rates are experienced at the different solidification fronts during pulsed laser welding, and different solidification modes and structures may result from these local variations.

In relation to pulsed laser welding parameters, if the metal melts and solidifies as a function of the pulse width, the solidification rates should be quite large. Given that the solidification time during pulsed laser welding is on the order of 20 ms after the pulse has completed [19], the solidification rate for the weld should be on the order of 50 mm/s (provided the pulsing frequency and pulse width is sufficiently low, as in the current case). Looking back to Figure 7, it is easily seen that the predicted solidification mode should be either fully austenite, primary ferrite with a massive transformation to austenite, or a combination of both (if mixing is non-uniform). Figure 8 seemed, however, to indicate that the solidification mode was either austenite, austenite with eutectic ferrite, or ferrite with peritectic/eutectic austenite. Thus, in the current case, Figure 7 over-predicts the dependence of primary solidification on solidification rate. In other words, the nose of the primary ferrite with peritectic/eutectic austenite should move upward to higher solidification rates for the current alloys/welding conditions. Nonetheless, Figure 7 does present a good starting point for predicting the primary solidification mode, and further work should be done to better define such a primary solidification mode map.

Finally, it should be noted that solidification cracking needs not only a crack-susceptible microstructure, but also sufficient tensile stress to drive a crack open. Certainly, a difference in shrinkage (and perhaps thermal) stress exists when comparing the conduction mode and keyhole mode welds. The resultant shape of the keyhole mode weld lends itself to higher shrinkage stress. The difference in stress, however, was not quantified nor studied in this investigation.

Summary

The most interesting part of this work is that two "weldable" alloys (*i.e.*, alloys which when autogenously welded, will have no apparent cracking) are welded together, a crack susceptible weld metal composition may result. Two different heats of UNS S30403 (304L stainless steel) when welded may easily fall into this category, as seen in the current investigation. Although this has previously been alluded to by Lippold[15], the modified Suutala diagram with a tie-line between two compositions depicts this well, as seen in Figure 6. By utilizing a tie line in these types of diagrams, useful information may be obtained about the potential crack susceptibility of the resulting weld metal. In addition, non-uniform mixing behavior may be observed in pulsed laser beam welds when welding in conduction mode with small pulse frequencies. However, this non-uniform mixing may be beneficial, as in the current case, when solidification cracking in the weld metal was avoided Drastic changes in weld metal composition in fact will influence the primary solidification mode of either dissimilar austenitic stainless steels (*e.g.* 304L to 316L) or different heats of similar material stainless steels (*e.g.* 304L to 304L) when welded.

References

1. J.C. Lippold, *Welding Journal*, 73, 129s-39s (1994)
2. F.C. Hull, *Welding Journal*, 67, 399s-409s (1967)
3. I. Masumoto, K. Tamaki, and M. Kutsuna, *Trans. JWS*, 41, 1306-14 (1972)
4. R. J. Arata, F. Matsuda, and S. Katayama, *Trans. JWRI*, 5, 35-51 (1976)
5. V. Kujanpaa, N. Suutala, T. Takalo, and T. Moisio, *Welding Research International*, 9, 55-76 (1979)
6. S.A. David, G.M. Goodwin, and D.N. Braski, *Welding Journal*, 58, 330s-36s (1979)
7. J.A. Brooks, *Trends in Welding Research in the U.S.*, pp.209-47, ASM Conference Proceedings, Materials Park, Ohio (1982)
8. J.A. Brooks and A.W. Thompson, *Int. Met. Reviews*, 36, 16-44 (1991)
9. J.A. Brooks, A.W. Thompson, and J.C. Williams, *Welding Journal,* 63, 71s-83s (1984)
10. N. Suutala, T. Takalo, and T. Moisio, *Metall. Trans.A*, 10A, 512-14 (1979)
11. A.L. Schaeffler, *Met. Prog*., 56, 680-680B (1949)
12. W. DeLong, G. Ostrom, and E. Szumachowski, *Welding Journal,* 35, 526s-33s (1956)
13. T.A. Siewert, C.N. McCowan and D.L. Olson, *Welding Journal*, 67, 289s-98s (1988)
14. D. Kotecki and T.A. Siewert, *Welding Journal*, 71, 171s-8s (1992)
15. J.C. Lippold, *Welding Journal*, 64, 127s-36s (1985)
16. J.W. Elmer, S.M. Allen, and T.W. Eager, *Metall. Trans. A*, 20A, 2117-30 (1989)
17. S.A. David, J.M. Vitek, and T.L. Hebble, *Welding Journal*, 66, 289s-300s (1987)
18. S. Katayama and A. Matsunawa, *Proceedings of the Materials Processing Symposium -ICALEO '84*, pp. 60-7 LIA-Laser Institute of America, Toledo, Ohio (1985)
19. T. Zacharia, S.A. David, J.M Vitek, and T. Debroy, *Metall. Trans. A*, 20A, 957-67 (1989)

Acknowledgements

This work was supported under the auspices of the United States Department of Energy at Los Alamos National Laboratory under contract number W-7405-ENG-36. The authors would like to acknowledge Mr. George Keel for performing the laser welding. The authors would also like to thank Mr. John Milewski, Mr. Gary Lewis, Dr. Martin Piltch and Dr. Paul Burgardt for many useful discussions.